



Combined Upper Limit on Standard Model Higgs Boson Production for Winter 2009

The CDF Collaboration
URL <http://www-cdf.fnal.gov>
(Dated: January 31, 2009)

This note describes a combination of searches for the Standard Model Higgs boson at CDF. The six major analyses combined are the $WH \rightarrow \ell\nu b\bar{b}$ channels, the $WH + ZH \rightarrow \cancel{E}_T + bb$ channels, the $ZH \rightarrow \ell^+\ell^- b\bar{b}$ channels, the $H \rightarrow \tau^+\tau^-$ channel, the $H \rightarrow W^+W^- \rightarrow \ell^+\nu_\ell\ell'^-\bar{\nu}_{\ell'}$ channels, and the $WH \rightarrow WW^+W^-$ channel. The integrated luminosity for the channels varies between 2.0 fb^{-1} and 3.0 fb^{-1} . The 95% CL upper limit on $R = \sigma_H/\sigma_{H,SM}$ is computed as a function of m_H from 100 to 200 GeV/c^2 in steps of $5 \text{ GeV}/c^2$, assuming Standard Model decay branching fractions of the Higgs boson and that the ratios of the rates for the WH , ZH , $gg \rightarrow H$ and vector-boson fusion $qq \rightarrow Hqq$ production mechanisms are those predicted by the Standard Model. The results are in good agreement with those expected in the background-only hypothesis, and the observed (expected) limits on R are 3.76 (3.17) and 1.56 (1.75) at Higgs boson masses of 115 and 160 GeV/c^2 , respectively.

Preliminary Results for Winter 2009 Conferences

I. INTRODUCTION

A combination of the different Higgs search analysis results provides many advantages. Since the decay branching ratios of the Standard Model (SM) Higgs boson are strong functions of its mass m_H , the different search channels contribute in a complementary way to the sensitivity at different m_H . Some analyses seek the Higgs boson in the same decay mode but with different production mechanisms, and hence require separate treatments of the signals and backgrounds. Since these analyses all seek the same particle, the best results arise in combination.

A previous combination [1] has been performed using the results of the five main searches for the Standard Model Higgs boson at CDF, the $WH \rightarrow \ell\nu b\bar{b}$ channels, the $WH + ZH \rightarrow \cancel{E}_T + b\bar{b}$ channels, the $ZH \rightarrow \ell^+\ell^-b\bar{b}$ channels, the $H \rightarrow \tau^+\tau^-$ channel, and the $H \rightarrow W^+W^- \rightarrow \ell^+\nu_\ell\ell'^-\bar{\nu}_{\ell'}$ channels. This note presents an update of the combination, using newly released results for all of the above channels, except the $H \rightarrow \tau^+\tau^-$ channel [2] and the $H \rightarrow W^+W^- \rightarrow \ell^+\nu_\ell\ell'^-\bar{\nu}_{\ell'}$ channels [3] which remain stable. The analyses include data up to 3 fb^{-1} , and many analysis improvements, the most important of which are summarized below. The analyzed luminosities and references to the documentation are provided in Table I.

In order to combine the results of the six search analyses, assumptions must be made about the model to be tested. The model tested by the individual analyses' notes is a model in which Standard Model Higgs boson production proceeds, but is enhanced, in all channels, by a factor of R in the cross section. The decay branching fractions and the width of the invariant mass distribution of the Higgs boson are assumed to be those predicted by the Standard Model. Exotic models which change the Higgs boson production cross section may not follow this pattern. If a fourth generation of fermions exists, for example, it would enhance the $gg \rightarrow H$ production cross section by a factor of roughly 9 [4], but would not enhance the WH and ZH associated production mechanisms. The Standard Model production cross sections and decay branching ratios used in this combination are the same as those used in the previous combination [1], with an update to the theoretical prediction of the $gg \rightarrow H$ production cross section due to previously ignored two-loop electroweak contributions [5]. These corrections amount to an upwards correction of the $gg \rightarrow H$ production cross section of up to 8% near $m_H = 2M_W$, and are assumed to factorize with respect to the NNLO QCD corrections already computed [6] and used in the previous combination. The cross sections used are reproduced in Table II. The cross sections listed in [6] are on a coarser mass grid than desired, and so MCFM [7] has been used to compute the remaining required cross sections, and has been found to agree well with those in [6]. The decay branching ratios are computed with HDECAY [8].

Many updates and improvements have been made to the channels since the previous combination [1], and are listed below.

- The $WH \rightarrow \ell\nu b\bar{b}$ channels using 2.7 fb^{-1} of integrated luminosity have been analyzed with two parallel analysis methods, a neural net [9] and a boosted decision tree with matrix-element inputs [10]. Each event in the data and the Monte Carlo passing an event selection requiring a lepton, missing transverse energy, and two or three jets, at least one of which must be b -tagged, is given a discriminant value by both of the analysis methods. These discriminant values are then used as inputs to a neuro-evolution technique to produce a single combined together using a neuro-evolution technique [11]. There are six total channels in this group, split by b -tag category and the lepton category. The three b -tag categories are: two tight SECVTX tags, one SECVTX tag and one JetProb (but not SECVTX) tag, and one SECVTX tag with no tag on the other jet. The two lepton categories are: triggered electron or muon candidates and isolated tracks. Separate neuro-evolution networks were trained to combine the NN and MEBDT analyses at each value of m_H on the test grid, to separate the $WH \rightarrow \ell\nu b\bar{b}$ signal from the backgrounds.
- The $WH + ZH \rightarrow \cancel{E}_T + b\bar{b}$ analysis is analyzed with 2.1 fb^{-1} of data [12], with a new analysis. The improvements include optimization of the discriminants for 2-jet and 3-jet events separately, and the addition of a trackMET NN to further separate events with fake missing E_T from the signal. The dominant QCD background is rejected with a separate NN before the final signal discriminant is formed. The data are grouped into three channels based on the tag status of the two jets. The b -tag categories are: two tight SECVTX tags, one SECVTX tag and one JetProb (but not SECVTX) tag, and one SECVTX tag with no tag on the other jet. The $ZH \rightarrow \ell^+\ell^-b\bar{b}$ signal has been added in, to count acceptance for events in which both leptons fail to reconstruct or pass selection requirements.
- The $ZH \rightarrow \ell^+\ell^-b\bar{b}$ channels [13] have been updated to 2.7 fb^{-1} of data, and the lepton selections have been loosened. This analysis carries forwards the two-dimensional neural network approach used previously, with an innovative jet-energy correction technique using a neural network and assignment of the \cancel{E}_T to the jets. The selected events are grouped into three analysis channels based on the b -tag category. These are: two tight SECVTX tags, one loose SECVTX tag and one JetProb tag (but not falling in the two-tight category), and one tight SECVTX tag (and also not falling in either of the other categories). The discriminant variables are

two neural nets designed to separate the Higgs boson signal from Z +jets and $t\bar{t}$, respectively, and limits are computed from two-dimensional histograms of these variables.

- The $H \rightarrow W^+W^- \rightarrow \ell^+\nu_\ell\ell'^-\bar{\nu}_{\ell'}$ channels are analyzed with 3.0 fb^{-1} [3], and use largely the same results as [1]. The DY templates have been updated. Four sources of signal are considered: $gg \rightarrow H$, WH associated production, ZH associated production, and vector boson fusion $qq \rightarrow qqH$, each assuming $H \rightarrow W^+W^- \rightarrow \ell^+\nu_\ell\ell'^-\bar{\nu}_{\ell'}$. In order to maximize the acceptance and separation of the signals from the SM backgrounds, dominated by nonresonant W^+W^- production, three separate analysis channels are considered: leptons+ \cancel{E}_T +zero jets, one jet, or two or more jets. A combined neural network and matrix element approach is used.

The mass grid for the $H \rightarrow W^+W^- \rightarrow \ell^+\nu_\ell\ell'^-\bar{\nu}_{\ell'}$ channels is in $5 \text{ GeV}/c^2$ steps between $m_H = 140 \text{ GeV}/c^2$ and $180 \text{ GeV}/c^2$, and in $10 \text{ GeV}/c^2$ steps outside that interval. As the combination requires a $5 \text{ GeV}/c^2$ step everywhere, the results have been interpolated for the test mass points 100, 105, 115, 125, and $135 \text{ GeV}/c^2$ by starting the signal, background and data histograms from the nearest supplied point with a test mass heavier than the one desired. The signal histograms (separately supplied for each of the four signal processes) are then scaled by the ratios of the production cross section and the decay branching ratio for $H \rightarrow W^+W^-$, and a separate two-loop EW correction is applied. This method is approximate because it does not interpolate the acceptance. Results at $m_H = 185$ and $195 \text{ GeV}/c^2$ are not quoted here since the $H \rightarrow W^+W^- \rightarrow \ell^+\nu_\ell\ell'^-\bar{\nu}_{\ell'}$ channels are the only ones to contribute, and these mass points were not included in the search. For the lower mass points, the $H \rightarrow b\bar{b}$ searches dominate the sensitivity. The same interpolation scheme is applied to the $H \rightarrow \tau^+\tau^-$ channel for the missing points at 125, 135, and $145 \text{ GeV}/c^2$.

- A new $WH \rightarrow WW^+W^-$ like-sign dilepton channel is included in the combination, using a boosted decision-tree analysis [14], including 2.7 fb^{-1} of data.

II. COMBINATION METHOD

A Bayesian technique is used to compute the observed and expected upper limits on R . The prior is flat in the product of R and the total expected signal yield after all efficiencies and acceptances are taken into account. This prior was used in the previous combination [1].

A. Common Parameter Alignment

The individual channel analyses listed above require theoretical input in the form of kinematic distributions from Monte Carlo (usually from leading-order generators with parton shower models), and higher-order predictions of inclusive cross sections. The method of inclusion of systematic uncertainties, described below, takes advantage of shared dependence on common parameters, such as the luminosity, the $t\bar{t}$ and single-top cross sections, the diboson cross sections and the vector-boson-plus-heavy-flavor-jets K factor relative to the Monte Carlo prediction.

The individual analyses use an older prediction of the $t\bar{t}$ cross section, 6.7 pb [16], assuming $m_t = 175 \text{ GeV}/c^2$. The analyses also use single top theoretical predictions [17] evaluated at $m_t = 175 \text{ GeV}/c^2$, $\sigma_s = 0.88 \text{ pb}$ for the s -channel production, and $\sigma_t = 1.96 \text{ pb}$ for t -channel production. In discussions with D0, we choose to shift $\sigma_{t\bar{t}}$ to its value at $m_t = 172.4 \pm 1.2 \text{ GeV}/c^2$ [18], and to use newer, higher-order calculations [19]. The channels' background templates are evaluated with $m_t = 175 \text{ GeV}/c^2$, but since the kinematics are not expected to be strongly dependent on m_t , particularly in advanced discriminants designed to separate Higgs boson events from backgrounds, only the cross section has been adjusted. We use a value of $\sigma_{t\bar{t}} = 7.794 \text{ pb}$, with an uncertainty of 3.9% due to the uncertainty on m_t , 5.3% due to the factorization and renormalization scale, and 2.9% from PDF uncertainty. The single top cross sections [20] are, for the s -channel, $1.083 \text{ pb} \pm 3.2\% (m_t) \pm 3.7\% (\text{scale}) \pm 1.9\% (\text{PDF})$, and for the t -channel, $2.295 \text{ pb} \pm 1.9\% (m_t) \pm 1.3\% (\text{scale}) \pm 5.2\% (\text{PDF})$. The templates from each channel have been scaled by the appropriate ratios of cross sections to unify the predictions. The above theoretical uncertainties are applied in place of those supplied by the analyses. The scale and PDF uncertainties are taken to be uncorrelated between the three processes.

The W, Z +heavy-flavor K -factors are correlated between the $WH \rightarrow \ell\nu b\bar{b}$ and the $ZH \rightarrow \ell^+\ell^-b\bar{b}$ channels, but these are considered uncorrelated with the $WH + ZH \rightarrow \cancel{E}_T + b\bar{b}$ channels, as the former use ALPGEN [21] to model W, Z +heavy-flavor events, and the latter use Pythia [22]. This decorrelation is conservative since the common handling of shared systematic uncertainties allows one channel's data to constrain another channel's background, and if the K -factors or other central values are not aligned, sharing a common uncertainty is an aggressive procedure.

The diboson processes WW, WZ and ZZ have been assigned a common theoretical uncertainty of 11.5%, shared across all channels.

The signal cross section uncertainties [6] have been unified across channels. We assign a 10% uncertainty to the $gg \rightarrow H$ production cross section, a 10% uncertainty on vector-boson fusion, and a 5% uncertainty on WH and ZH production (correlated between WH and ZH), independent of m_H . The theoretical uncertainties on the Higgs boson production mechanisms are considered to be independent of each other and of all other uncertainties.

The luminosity uncertainties are split into a ‘‘Luminosity’’ category which refers to our uncertainty on the inelastic $p\bar{p}$ cross-section, and a ‘‘Luminosity Monitor’’ category, which refers to CDF-specific luminosity uncertainty. The ‘‘Luminosity’’ category, taken to be 3.8% and the ‘‘Luminosity Monitor’’ uncertainty is taken to be 4.4% for all templates of signal and background that are normalized to theoretical predictions times the luminosity measurement. Components that are already normalized to data observations in control samples do not have this uncertainty. This breakdown is necessary for proper correlation with D0’s luminosity uncertainty.

B. Systematic Uncertainties

Systematic uncertainties are incorporated by marginalizing the likelihood function over variations in the uncertain parameters, called ‘‘nuisance parameters’’. Each nuisance parameter is considered to be independent of the others, but each one may have an effect on any of the signal or background predictions in any of the channels. Nuisance parameters included in this combination include the integrated luminosity, the jet energy scale, the b-tag efficiency scale factor, mistag uncertainties, the lepton trigger efficiencies, the lepton identification efficiencies and fake rates, Monte Carlo generator differences, uncertainties due to missing higher-order terms in the signal and background MC predictions, Monte Carlo modeling of ISR, FSR and PDFs, background production cross sections for $t\bar{t}$, diboson, and other backgrounds, mistag matrix uncertainties, the heavy-flavor fraction in W +jets, and the uncertainties in non- W contributions. Full listings of the nuisance parameters affecting these analyses are summarized in tables for each channel at the end of this note. The nuisance parameters affect the predicted rates of different signal and background processes, and some nuisance parameters have shape uncertainties associated with them as well.

Rate uncertainties on template histograms are incorporated by multiplying the dependences of each rate on each nuisance parameter.

$$s_{\text{varied}} = s_{\text{central}} \prod_{i=1}^{n_{\text{params}}} (1 + f_i \eta_i) \quad (1)$$

where s_{varied} is the systematically varied normalization scale factor on a particular prediction histogram (signal or background) in a channel, s_{central} is the central-value normalization scale factor for that template, f_i is the relative uncertainty on s due to nuisance parameter i , and η_i is the random truncated-Gaussian-distributed nuisance parameter. Indices for the analysis channel and background or signal source template have been suppressed. The multiplicative technique used here means that the nuisance parameter truncations are all independent of each other.

Shape uncertainties are handled by varying the template shapes according to the nuisance parameters η_i . Systematically-varied shapes are supplied by the analysis teams as histograms which are generated with systematically varied parameters. These parameters may be the same ones as are responsible for the rate variations, and the variations are taken to be correlated. For example, a jet energy scale variation affects both the rate and the shape of most expected signal histograms. All analyses now use histograms of sophisticated multivariate discriminants in order to present their results, and the left-right template shifting interpolation is no longer used to incorporate shape uncertainties. Instead, the simpler method of linearly interpolating between the central value shapes and the systematically varied shapes in each bin according to the value of the nuisance parameter. Shape systematics are compounded by adding linearly the changes due to several shape variations in each bin. Shape systematics are extrapolated beyond the usual $\pm 1\sigma$ variations provided by the analysis teams. If a particular choice of shape variations results in a negative prediction for any signal or background component in any bin, then the prediction for that component is set to zero in that bin, but it does not prevent that variation from being applied to other bins. It is recommended that in the future analyzers investigate what multi-sigma variations in systematic parameters do to the predicted final discriminant shapes.

Another source of rate and shape variation is limited MC statistics in each bin of the template histograms. Each analysis supplies histograms along with their independent uncertainties in ROOT histogram objects. These uncertainties do not include the correlated rate and shape uncertainties described above, but are meant to cover the effects of MC statistics (or data statistics, if data control regions are used to predict the composition of the selected events in the signal region).

C. Numerical Integration

The space spanned by the nuisance parameters has a very large dimension – 52 uncertain parameters in all. The posterior calculation integrates over all possible values of the nuisance parameters, weighted by their priors. In the previous combination [1], the of [?] is adopted – the nuisance parameter marginalization is done by Monte Carlo integration. Points within the nuisance parameter space are selected randomly using truncated Gaussian distributions with unit width (before truncation). The domain of each nuisance parameter is truncated in order to keep the prediction of the rate of each template non-negative; no other truncation is applied.

The number of nuisance parameters increases as more search channels are added, and the gap between the prior information about a nuisance parameter and what can be determined from the data about a particular nuisance parameter has been increasing as well, for certain key nuisance parameters. For example, the W, Z +Heavy Flavor rate has an uncertainty of $\sim 40\%$, mainly by fitting heavy-flavor fractions to control samples in the data that do not overlap with the W, Z +2-jet samples used for the signal extraction. But large amounts of data in the W, Z +2-jet samples have been accumulated, and these constrain the W, Z +Heavy Flavor rate much more precisely than the priors – by approximately a factor of four. This has a large effect on the random-sampling integration method because most samplings of the W, Z +Heavy Flavor rate parameter produce predictions that are at large variance with the data observations, and result in very small values of the likelihood, and contribute very little to the integral. One or two such parameters do not present a computational challenge, but the presence of many such parameters has the effect that nearly all samples of the systematic errors contribute very little, and one or two samples in a large run will contribute nearly all of the weight of the integral.

A new approach has been taken to perform the integrals over the nuisance parameters, that of Markov Chain Monte Carlo integration. The Metropolis-Hastings algorithm [23] is used. This algorithm has found broad use in high-dimensional integrals elsewhere, particularly in the application of Bayesian statistics. All integrals start at the point in nuisance parameter space at which all parameters are zero (corresponding to the central values of all predictions). A proposal function determines where to step next in nuisance parameter space, and the Markov Chain moves to the proposed point if it has a higher value of the likelihood or if a random number between 0 and 1 is less than the ratio of the likelihood at the new point divided by the likelihood at the old point. This algorithm focuses on parts of parameter space for which the integrand is largest, thus saving computational resources and producing more reliable results in shorter times.

All limits are quoted at the 95% confidence level. Expected limits are quoted as the median limit expected in a sample (1000) of background-only pseudoexperiments, and the $\pm 1, 2\sigma$ variations. On each pseudoexperiment, new values of the nuisance parameters are drawn from the Gaussian distributions specified in the systematic uncertainty tables, and Poisson random pseudodata are drawn from the systematically smeared predictions. In order to reduce the amount of CPU used in the combination and to get more reliable $\pm 2\sigma$ expected limit estimations, the distribution of limits in the pseudoexperiments is fit to the density function $d(R)$:

$$d(R) = p_1(R - p_2)^{p_3} e^{-p_4 R}, \quad (2)$$

where p_1, p_2, p_3 , and p_4 are freely-floating fit parameters. This function is then integrated to obtain the desired quantiles, which correspond to 2.275% of limits being below the -2σ limit expectation in a large ensemble of background-only outcomes, 16% being below the -1σ limit expectation, 50% being below the median expectation, 84% being below the $+1\sigma$ expectation, and 97.725% being below the $+2\sigma$ expectation.

III. INDIVIDUAL CHANNEL LIMITS

In order to validate the input histogram preparation and the combination method, the observed and expected limits have been recomputed for each of the contributing channels before the final combination is performed. The rates and systematic uncertainties of each of the signal contributions and the backgrounds are compared with the available documentation. For the individual channel limits, 50000 Monte Carlo samples are performed for the observed limit, and only 25 pseudoexperiments were run for the expected limits. Tables at the end of this note compare the observed and expected limits blessed by the analysis teams and the reproductions computed here. In most cases, the agreement is exquisite, since the same programs are used to compute the individual limits as is used to combine many channels together.

IV. COMBINATION RESULTS

The results of the combination are given in Table XXI, and in Figure 1. Figure 2 compares the observed and expected limits obtained in combination with those of the individual analyses. The SM Higgs mass limit from LEP [24] is included in the plots. The same procedure for computing the individual channel limits is applied, but a joint likelihood is formed for all channels together, and variations of shared nuisance parameters, which affect both rates and shapes, are all performed with 100% correlations between parameters with the same name, and 0% correlation between parameters with different names.

The posterior of the combined results is shown in Figures 3 and 4 for each value of m_H between 100 and 200 GeV/c^2 in 5 GeV/c^2 steps. The distributions of the limits expected in background-only pseudoexperiments are shown in Figures 5 and 6.

To visualize the combined results better, the data are collected from all channels and are classified by the signal-to-background ratio in each bin. Bins of nearby s/b are collected together, and plotted vs $\log_{10}(s/b)$ in Figures 7 for $m_H = 115$ and $160 \text{ GeV}/c^2$. The data are then integrated from the high s/b side towards the lower, and the data counts are shown in Figure 7 for the same two Higgs boson masses. These integrals answer the question of how many events were observed, compared with the signal and background predictions. Because many bins of different s/b are used to make the final limit, there is an arbitrary choice of where to put a cut to answer that question. Figure 7 shows that answer for several high- s/b cuts. Drawbacks of this representation are that systematic uncertainties are not shown.

V. PROJECTIONS

As data are accumulated, the sensitivity of the searches is expected to increase. A naive extrapolation of the sensitivity is to scale the median expected limit with $1/\sqrt{\int L dt}$. This approximation makes several assumptions: 1) that the background levels in the high s/b bins is sufficiently large that the distribution of data events is expected to be in the Gaussian regime of the Poisson distribution, 2) that the systematic uncertainties scale with $1/\sqrt{\int L dt}$ for each channel, 3) that the analysis techniques remain constant, 4) that the detector performance remains constant and also does not degrade with increased instantaneous luminosity, and 5) that the tested models do not change. The experience on CDF is that the detector performance remains nearly constant, with only a mild drop due to the increased instantaneous luminosity. Larger control samples allow better constraints on systematic uncertainties, and also can be used to test extrapolations into signal regions by refining the definitions of the control samples. Analysis improvements such as increasing acceptance by exploiting previously unused trigger paths and event topologies, as well as improved separation of signal from background through the use of multivariate techniques and combinations of multivariate techniques have brought about increases in sensitivity that surpass what is expected from the $1/\sqrt{\int L dt}$ dependence alone. The comparison of the achieved expected limits and the $1/\sqrt{\int L dt}$ extrapolations is shown in Figure 8 for $m_H = 115$ and $160 \text{ GeV}/c^2$.

In Figure 8, the integrated luminosity at which to place a point is a simple unweighted average of the contributing analyses' integrated luminosities. For the $m_H = 115 \text{ GeV}/c^2$ point, the the $WH \rightarrow \ell\nu b\bar{b}$, the $WH + ZH \rightarrow \cancel{E}_T + b\bar{b}$, the $ZH \rightarrow \ell^+\ell^-b\bar{b}$, and the $H \rightarrow \tau^+\tau^-$ channels' luminosities are averaged, when they were available and contributed. The $H \rightarrow \tau^+\tau^-$ channel did not exist before Winter 2008. For the $m_H = 160 \text{ GeV}/c^2$ points, only the $H \rightarrow W^+W^- \rightarrow \ell^+\nu_\ell\ell'^-\bar{\nu}_{\ell'}$ luminosity is used. In the $m_H = 160 \text{ GeV}/c^2$ plot, the limits from Summer 2004 and Summer 2005 have been scaled to use the NNLO $gg \rightarrow H$ cross section which is approximately 50% larger than the NLO cross section, which was used in the original analyses. Only the ICHEP 2008 point includes the scaling using the new 2-loop electroweak diagrams, however.

The projection figures include estimations of how much the sensitivity could be improved over time as work is done on the analyses. The estimations were made in late 2007, based on the Summer 2007 estimations of sensitivity. A factor of 1.5 in the expected limit was estimated to be attainable with improvements known to exist but not yet in the analyses, and a further factor of 1.5 was estimated from ideas that had yet to be tried. Both of these curves are shown, as the top and bottom edges of light orange bands in the figures. For both the low-mass and high-mass searches, the first factor of 1.5 has already been achieved.

Figure 9 shows the same projections, but the expected limits have all been divided by $\sqrt{2}$ to simulate the effect of combining with D0, assuming performance equal to CDF's. Figure 10 shows the chances of observing a 2σ excess or 3σ evidence as a function of m_H , assuming a Higgs boson is present and the production cross section and decay parameters are as predicted by the SM. CDF and D0 are assumed to contribute equally, and the performance level

is shown both for the currently achieved performance level and also for an additional factor of 1.5. Two luminosity scenarios are considered, 5 fb^{-1} and 10 fb^{-1} of analyzed luminosity per experiment. Only the sensitivity estimated by the signal and background templates and their systematic uncertainties is shown in these plots, and no account is taken of the data already observed. In particular, a deficit in the Tevatron combination at $m_H = 170 \text{ GeV}/c^2$ allows the exclusion of that mass [25], and so the chances of observing an excess or evidence are lessened when considering the data. Furthermore, even if a SM Higgs boson is nonetheless assumed to exist at $m_H = 170 \text{ GeV}/c^2$, it will take more data and additional luck in order to accumulate enough candidates to amass the evidence after the unlucky downward fluctuation.

VI. ACKNOWLEDGEMENTS

The authors would like to thank the Higgs Discovery group, particularly those who provided the results for combination.

-
- [1] W.-M. Yao, T. Junk, N. Krumnack CDF Note 9502 (2008).
 - [2] CDF Collaboration, CDF Note 9248 (2008).
 - [3] CDF Collaboration, CDF Note 9500 (2008).
 - [4] E. Arik, O. Cakir, S. A. Cetin and S. Sultansoy, *Acta Phys. Polon.* **B37**:2839-2850 (2006). Available online as [arXiv:hep-ph/0502050](https://arxiv.org/abs/hep-ph/0502050).
 - [5] U. Aglietti, R. Bonciani, G. Degrassi, A. Vicini, "Two-loop electroweak corrections to Higgs production in proton-proton collisions", [arXiv:hep-ph/0610033v1](https://arxiv.org/abs/hep-ph/0610033v1) (2006).
 - [6] TeV4LHC Higgs working group at <http://maltoni.home.cern.ch/maltoni/TeV4LHC/SM.html>.
 - [7] J.M. Campbell, R.K. Ellis, *Phys. Rev. D* **62**:114012 (2000), [hep-ph/0006304](https://arxiv.org/abs/hep-ph/0006304). See also <http://mcfm.fnal.gov/index.html>.
 - [8] A. Djouadi, K.Kalinowski and M. Spira, *Comp. Phys. Commun.* **108C** 56 (1998).
 - [9] CDF Collaboration, CDF Note 9468 (2008).
 - [10] CDF Collaboration, CDF Note 9463 (2008).
 - [11] CDF Collaboration, CDF Note 9596 (2008).
 - [12] CDF Collaboration, CDF Note 9642 (2008).
 - [13] CDF Collaboration, CDF Note 9665 (2008).
 - [14] CDF Collaboration, CDF Note 7307 (2008). This combination is done with the analysis described in Version 3.0 of this note.
 - [15] C. Blocker, J. Conway, L. Demortier, J. Heinrich, T. Junk, L. Lyons, G. Punzi, CDF Note 7739 (2005).
 - [16] M. Cacciari, S. Frixione, M. L. Mangano, P. Nason and G. Ridolfi, *JHEP* **0809**, 127 (2008) [[arXiv:0804.2800](https://arxiv.org/abs/0804.2800) [hep-ph]].
 - [17] B. W. Harris, E. Laenen, L. Phaf, Z. Sullivan and S. Weinzierl, *Phys. Rev. D* **66**, 054024 (2002) [[arXiv:hep-ph/0207055](https://arxiv.org/abs/hep-ph/0207055)].
 - [18] The Tevatron Electroweak Working Group, for the CDF, D0 Collaborations, "Combination of CDF and D0 Results on the Mass of the Top Quark", [arXiv:0808.1089v1](https://arxiv.org/abs/0808.1089v1) [hep-ex] (2008).
 - [19] S. Moch and P. Uwer, *Nucl. Phys. Proc. Suppl.* **183**, 75 (2008) [[arXiv:0807.2794](https://arxiv.org/abs/0807.2794) [hep-ph]]; N. Kidonakis and R. Vogt, *Phys. Rev. D* **78**, 074005 (2008) [[arXiv:0805.3844](https://arxiv.org/abs/0805.3844) [hep-ph]].
 - [20] N. Kidonakis, *Phys. Rev. D* **74**, 114012 (2006) [[arXiv:hep-ph/0609287](https://arxiv.org/abs/hep-ph/0609287)].
 - [21] M.L. Mangano, M. Moretti, F. Piccinini, R. Pittau, A. Polosa, *JHEP* **0307**:001; [hep-ph/0206293](https://arxiv.org/abs/hep-ph/0206293) (2003).
 - [22] T. Sjostrand, L. Lonnblad and S. Mrenna, [arXiv:hep-ph/0108264](https://arxiv.org/abs/hep-ph/0108264) (2001); T. Sjostrand, P. Eden, C. Friberg, L. Lonnblad, G. Miu, S. Mrenna and E. Norrbin, *Comput. Phys. Commun.* **135**, 238 (2001). [[arXiv:hep-ph/0010017](https://arxiv.org/abs/hep-ph/0010017)].
 - [23] N. Metropolis, A.W. Rosenbluth, M.N. Rosenbluth, A.H. Teller, and E. Teller. "Equations of State Calculations by Fast Computing Machines". *Journal of Chemical Physics*, 21(6):1087-1092, (1953). W.K. Hastings. "Monte Carlo Sampling Methods Using Markov Chains and Their Applications", *Biometrika*, 57(1):97-109, (1970).
 - [24] The ALEPH, DELPHI, L3 and OPAL Collaborations, and the LEP Higgs Working Group, *Phys. Lett. B* **565**, 61 (2003).
 - [25] The CDF and D0 Collaborations, and the Tevatron New Phenomena and Higgs Working Group, [arXiv:0808.0534](https://arxiv.org/abs/0808.0534) [hep-ex] (2008).

TABLE I: Analyzed integrated luminosities and references for the four main CDF SM Higgs search channels combined in this note

Channel	$\int \mathcal{L} dt$ (fb $^{-1}$)	Reference
$WH \rightarrow \ell\nu b\bar{b}$ (triggered leptons+isotr)	2.7	[9–11]
$ZH \rightarrow \nu\bar{\nu} b\bar{b}$	2.1	[12]
$ZH \rightarrow \ell^+\ell^- b\bar{b}$	2.7	[13]
$H \rightarrow \tau^+\tau^-$	2.0	[2]
$H \rightarrow W^+W^- \rightarrow \ell^+\nu_\ell\ell'^-\bar{\nu}_{\ell'}$	3.0	[3]
$WH \rightarrow WW^+W^-$	2.7	[14]

TABLE II: The (N)NLO production cross sections and decay branching fractions for the SM Higgs boson assumed for the combination

m_H (GeV/ c^2)	$\sigma_{gg\rightarrow H}$ (fb)	σ_{WH} (fb)	σ_{ZH} (fb)	σ_{VBF} (fb)	$B(H \rightarrow b\bar{b})$ (%)	$B(H \rightarrow \tau^+\tau^-)$ (%)	$B(H \rightarrow W^+W^-)$ (%)
100	1689.9	286.1	166.7	99.5	81.21	7.924	1.009
105	1497.1	244.6	144.0	93.3	79.57	7.838	2.216
110	1332.0	209.2	124.3	87.1	77.02	7.656	4.411
115	1188.1	178.8	107.4	79.07	73.22	7.340	7.974
120	1057.5	152.9	92.7	71.65	67.89	6.861	13.20
125	945.4	132.4	81.1	67.37	60.97	6.210	20.18
130	847.8	114.7	70.9	62.5	52.71	5.408	28.69
135	762.0	99.3	62.0	57.65	43.62	4.507	38.28
140	687.5	86.0	54.2	52.59	34.36	3.574	48.33
145	621.3	75.3	48.0	49.15	25.56	2.676	58.33
150	563.4	66.0	42.5	45.67	17.57	1.851	68.17
155	511.5	57.8	37.6	42.19	10.49	1.112	78.23
160	460.7	50.7	33.3	38.59	4.00	0.426	90.11
165	409.3	44.4	29.5	36.09	1.265	0.136	96.10
170	367.6	38.9	26.1	33.58	0.846	0.091	96.53
175	333.4	34.6	23.3	31.11	0.663	0.072	95.94
180	303.1	30.7	20.8	28.57	0.541	0.059	93.45
190	247.8	24.3	16.6	24.88	0.342	0.038	77.61
200	207.3	19.3	13.5	21.19	0.260	0.029	73.47

TABLE III: Systematic uncertainties for the $WH \rightarrow \ell\nu b\bar{b}$ analysis, for the SECVTX+JP channel and the double-SECVTX tag channel. Systematic uncertainties are listed by name, see the original references for a detailed explanation of their meaning and on how they are derived. Systematic uncertainties for the WH signal shown in this table are obtained for $m_H = 115 \text{ GeV}/c^2$. Uncertainties are relative, in percent and are symmetric unless otherwise indicated.

SECVTX+JP $WH \rightarrow \ell\nu b\bar{b}$
analysis.

Contribution	W+HF	Mistags	Top	Diboson	Non-W	WH
Luminosity ($\sigma_{\text{inel}}(p\bar{p})$)	0	0	3.8	3.8	0	3.8
Luminosity Monitor	0	0	4.4	4.4	0	4.4
Lepton ID	0	0	2	2	0	2
Jet Energy Scale	0	0	0	0	0	2
Mistag Rate	0	8.0	0	0	0	0
B-Tag Efficiency	0	0	9.1	9.1	0	9.1
$t\bar{t}$ Cross Section	0	0	10	0	0	0
Diboson Rate	0	0	0	11.5	0	0
Signal Cross Section	0	0	0	0	0	5
HF Fraction in W+jets	30.1	0	0	0	0	0
ISR+FSR+PDF	0	0	0	0	0	4.3
QCD Rate	0	0	0	0	40	0

Double-SECVTX Tagged $WH \rightarrow \ell\nu b\bar{b}$
analysis.

Contribution	W+HF	Mistags	Top	Diboson	Non-W	WH
Luminosity ($\sigma_{\text{inel}}(p\bar{p})$)	0	0	3.8	3.8	0	3.8
Luminosity Monitor	0	0	4.4	4.4	0	4.4
Lepton ID	0	0	2	2	0	2
Jet Energy Scale	0	0	0	0	0	2
Mistag Rate	0	9.0	0	0	0	0
B-Tag Efficiency	0	0	8.4	8.4	0	8.4
$t\bar{t}$ Cross Section	0	0	10	0	0	0
Diboson Rate	0	0	0	11.5	0	0
Signal Cross Section	0	0	0	0	0	5
HF Fraction in W+jets	30.1	0	0	0	0	0
ISR+FSR+PDF	0	0	0	0	0	5.6
QCD Rate	0	0	0	0	40	0

TABLE IV: Systematic uncertainties for the $WH \rightarrow \ell\nu b\bar{b}$ analysis, for the single-SECVTX tag channel. Systematic uncertainties are listed by name, see the original references for a detailed explanation of their meaning and on how they are derived. Systematic uncertainties for the WH signal shown in this table are obtained for $m_H = 115 \text{ GeV}/c^2$. Uncertainties are relative, in percent and are symmetric unless otherwise indicated.

Single-SECVTX tag $WH \rightarrow \ell\nu b\bar{b}$
analysis.

Contribution	W+HF	Mistags	Top	Diboson	Non-W	WH
Luminosity ($\sigma_{\text{inel}}(p\bar{p})$)	0	0	3.8	3.8	0	3.8
Luminosity Monitor	0	0	4.4	4.4	0	4.4
Lepton ID	0	0	2	2	0	2
Jet Energy Scale	0	0	0	0	0	2
Mistag Rate	0	13.3	0	0	0	0
B-Tag Efficiency	0	0	3.5	3.5	0	3.5
$t\bar{t}$ Cross Section	0	0	10	0	0	0
Diboson Rate	0	0	0	11.5	0	0
Signal Cross Section	0	0	0	0	0	5
HF Fraction in W+jets	30.1	0	0	0	0	0
ISR+FSR+PDF	0	0	0	0	0	3.1
QCD Rate	0	0	0	0	40	0

TABLE V: Observed and expected limits for the six total $WH \rightarrow \ell\nu b\bar{b}$ channels: (double tag + SECVTX+JP, + single SECVTX) \times (single-tag and double-tag analyses combined). The observed and median expected limits in the background-only hypothesis are listed. Also listed are the limits from [11]. The limits are all given in units of $R = \sigma/\sigma_{SM}$, assuming SM branching fractions.

m_H (GeV/ c^2)	Observed limit/SM	median expected	CDF 9596 observed	CDF 9596 expected
100	3.45	3.74	3.27	3.54
105	3.63	3.96	3.56	3.80
110	4.99	4.29	4.87	4.14
115	5.68	4.92	5.59	4.81
120	5.93	6.36	5.93	5.91
125	8.04	7.46	7.96	7.18
130	8.61	8.90	8.89	8.72
135	12.76	12.78	13.2	12.2
140	22.29	17.60	26.5	17.5
145	39.74	27.05	42.2	25.6
150	70.25	42.69	75.5	40.5

TABLE VI: Systematic uncertainties $WH + ZH \rightarrow \cancel{E}_T + bb$, Double-SECVTX Channel. Systematic uncertainties are listed by name, see the original references for a detailed explanation of their meaning and on how they are derived. Systematic uncertainties for ZH and WH shown in this table are obtained for $m_H = 120$ GeV/ c^2 . Uncertainties are relative, in percent and are symmetric unless otherwise indicated.

	ZH	WH	Multijet	Top Pair	S. Top	Di-boson	W + h.f.	Z + h.f.
<i>Correlated uncertainties</i>								
Lumi($\sigma_{inel}(p\bar{p})$)	3.8%	3.8%		3.8%	3.8%	3.8%	3.8%	3.8%
Lumi Monitor	4.4%	4.4%		4.4%	4.4%	4.4%	4.4%	4.4%
Tagging SF	8.6%	8.6%		8.6%	8.6%	8.6%	8.6%	8.6%
Trigger Eff. (shape)	1.0%	1.2%	1.1%	0.7%	1.1%	1.6%	1.7%	1.3%
Lepton Veto	2.0%	2.0%		2.0%	2.0%	2.0%	2.0%	2.0%
PDF Acceptance	2.0%	2.0%		2.0%	2.0%	2.0%	2.0%	2.0%
JES (shape)	+3.0% -3.0%	+3.5% -4.7%	-4.0% +3.8%	+1.1% -1.1%	+2.4% -4.7%	+8.2% -6.1%	+7.3% -11.8%	+6.5% -8.3%
ISR		+4.4% +3.7%						
FSR		+1.8% +4.4%						
<i>Uncorrelated uncertainties</i>								
Cross-Section	5%	5%		10%	10%	11.5%	40%	40%
Multijet Norm. (shape)			20.6%					

TABLE VII: Systematic uncertainties $WH + ZH \rightarrow \cancel{E}_T + bb$, SECVTX+JP Channel. Systematic uncertainties are listed by name, see the original references for a detailed explanation of their meaning and on how they are derived. Systematic uncertainties for ZH and WH shown in this table are obtained for $m_H = 120$ GeV/ c^2 . Uncertainties are relative, in percent and are symmetric unless otherwise indicated.

	ZH	WH	Multijet	Top Pair	S. Top	Di-boson	W + h.f.	Z + h.f.
<i>Correlated uncertainties</i>								
Lumi($\sigma_{inel}(p\bar{p})$)	3.8%	3.8%		3.8%	3.8%	3.8%	3.8%	3.8%
Lumi Monitor	4.4%	4.4%		4.4%	4.4%	4.4%	4.4%	4.4%
Tagging SF	12.4%	12.4%		12.4%	12.4%	12.4%	12.4%	12.4%
Trigger Eff. (shape)	1.2%	1.3%	1.1%	0.7%	1.2%	1.2%	1.8%	1.3%
Lepton Veto	2.0%	2.0%		2.0%	2.0%	2.0%	2.0%	2.0%
PDF Acceptance	2.0%	2.0%		2.0%	2.0%	2.0%	2.0%	2.0%
JES (shape)	+3.7% -3.7%	+4.0% -4.0%	-5.4% +5.2%	+1.1% -0.7%	+4.2% -4.2%	+7.0% -7.0%	+1.3% -7.6%	+6.2% -7.1%
ISR		+1.4% -2.9%						
FSR		+5.3% +2.5%						
<i>Uncorrelated uncertainties</i>								
Cross-Section	5.0%	5.0%		10%	10%	11.5%	40%	40%
Multijet Norm. (shape)			15.6%					

TABLE VIII: Systematic uncertainties $WH + ZH \rightarrow \cancel{E}_T + bb$, Single SECVTX Tag Channel. Systematic uncertainties are listed by name, see the original references for a detailed explanation of their meaning and on how they are derived. Systematic uncertainties for ZH and WH shown in this table are obtained for $m_H = 120 \text{ GeV}/c^2$. Uncertainties are relative, in percent and are symmetric unless otherwise indicated.

	ZH	WH	Multijet	Top Pair	S. Top	Di-boson	W + h.f.	Z + h.f.
<i>Correlated uncertainties</i>								
Lumi($\sigma_{inel}(p\bar{p})$)	3.8%	3.8%		3.8%	3.8%	3.8%	3.8%	3.8%
Lumi Monitor	4.4%	4.4%		4.4%	4.4%	4.4%	4.4%	4.4%
Tagging SF	4.3%	4.3%		4.3%	4.3%	4.3%	4.3%	4.3%
Trigger Eff. (shape)	0.9%	1.1%	1.1%	0.7%	1.1%	1.3%	2.0%	1.4%
Lepton Veto	2.0%	2.0%		2.0%	2.0%	2.0%	2.0%	2.0%
PDF Acceptance	2.0%	2.0%		2.0%	2.0%	2.0%	2.0%	2.0%
JES (shape)	+3.8% -3.8%	+3.8% -3.8%	-5.2% +5.6%	+0.7% -0.8%	+4.6% -4.6%	+7.0% -5.6%	+12.4% -12.7%	+8.3% -8.1%
ISR		-1.0%						
FSR		-1.5% +2.0% -0.1%						
<i>Uncorrelated uncertainties</i>								
Cross-Section	5.0%	5.0%		10%	10%	11.5%	40%	40%
Multijet Norm. (shape)			5.5%					

TABLE IX: Observed and expected limits for the $WH + ZH \rightarrow \cancel{E}_T + b\bar{b}$ channels, with the single-tag and double-tag analyses combined. The observed and median expected limits are listed. Also listed are the limits from [12]. The limits are all given in units of $R = \sigma/\sigma_{SM}$, assuming SM branching fractions.

m_H (GeV/ c^2)	Observed limit/SM	median expected	CDF 9642 observed	CDF 9642 expected
100	6.07	4.97		
105	5.78	4.77	5.5	4.7
110	6.20	4.89	5.8	4.9
115	7.31	5.69	6.9	5.6
120	9.30	6.89	8.9	7.2
125	12.85	8.81	11.9	8.4
130	15.12	10.26	14.4	10.3
135	16.68	14.23	16.2	13.8
140	21.55	19.16	21.0	18.6
145	36.23	29.18	33.4	28.6
150	54.28	44.6	49.8	43.3

TABLE XII: Observed and expected limits for the $ZH \rightarrow \ell^+\ell^-b\bar{b}$ channels, with the single-tag and double-tag analyses combined. The observed and median expected limits are listed. Also listed are the limits from [13]. The limits are all given in units of $R = \sigma/\sigma_{SM}$, assuming SM branching fractions.

m_H (GeV/ c^2)	Observed limit/SM	median expected	CDF 9665 observed	CDF 9665 expected
100	6.35	8.76	6.0	8.92
105	5.46	8.78	5.4	8.85
110	6.77	9.36	6.6	9.3
115	7.27	9.95	7.1	9.9
120	8.69	11.88	8.6	12.2
125	10.95	14.12	11.1	13.8
130	14.10	18.10	13.4	17.4
135	18.65	24.43	18.3	23.3
140	28.12	33.49	27.1	34.3
145	44.17	51.43	44.0	51.7
150	70.55	86.08	68.5	83.4

TABLE XIII: Systematic uncertainties on the contributions for the $H \rightarrow \tau^+\tau^-$ channel. Systematic uncertainties are listed by name, see the original references for a detailed explanation of their meaning and on how they are derived. Uncertainties with provided shape systematics are labeled with “s”. Systematic uncertainties for H shown in this table are obtained for $m_H = 115$ GeV/ c^2 . Uncertainties are relative, in percent and are symmetric unless otherwise indicated. The systematic uncertainty called “Normalization” includes effects of the inelastic $p\bar{p}$ cross section, the luminosity monitor acceptance, and the lepton trigger acceptance. It is considered to be entirely correlated with the luminosity uncertainty.

Contribution	$Z/\gamma^* \rightarrow \tau\tau$	$Z/\gamma^* \rightarrow \ell\ell$	$t\bar{t}$	diboson	jet $\rightarrow \tau$	W+jet	WH	ZH	VBF	$gg \rightarrow H$
Luminosity	3.8	3.8	3.8	3.8	-	-	3.8	3.8	3.8	3.8
Luminosity Monitor	4.4	4.4	4.4	4.4	-	-	4.4	4.4	4.4	4.4
e, μ Trigger	1	1	1	1	-	-	1	1	1	1
τ Trigger	3	3	3	3	-	-	3	3	3	3
e, μ, τ ID	3	3	3	3	-	-	3	3	3	3
PDF Uncertainty	1	1	1	1	-	-	1	1	1	1
ISR/FSR	-	-	-	-	-	-	2/0	1/1	3/1	12/1
JES (shape)	16	13	2	10	-	-	3	3	4	14
Cross Section or Norm.	2	2	10	11.5	-	15	5	5	10	10
MC model	20	10	-	-	-	-	-	-	-	-

TABLE XIV: Observed and expected limits for the $H \rightarrow \tau^+\tau^-$ channel. The observed and median expected limits are listed. Also listed are the limits from [2]. The limits are all given in units of $R = \sigma/\sigma_{SM}$, assuming SM branching fractions.

m_H (GeV/ c^2)	Observed limit/SM	median expected	CDF 9179 observed	CDF 9179 expected
110	30.56	26.3	32.5	25.8
115	31.34	25.11	30.5	24.8
120	29.78	24.40	30.0	24.2
125	29.01	25.25	-	-
130	37.53	32.97	39.5	32.3
135	44.04	36.14	-	-
140	62.39	51.28	67.5	52.8
145	91.11	73.67	-	-
150	146.71	116.08	159.0	111.7

TABLE XVI: Systematic uncertainties on the contributions for CDF's $H \rightarrow W^+W^- \rightarrow \ell^\pm\ell^\mp$ channel with one jet. Systematic uncertainties are listed by name, see the original references for a detailed explanation of their meaning and on how they are derived. Systematic uncertainties for $gg \rightarrow H$ shown in this table are obtained for $m_H = 160 \text{ GeV}/c^2$. Uncertainties are relative, in percent and are symmetric unless otherwise indicated. Uncertainties in bold are correlated across jet bins but not across channels. Uncertainties in italics are correlated across jet bins and across appropriate channels.

Uncertainty Source	WW	WZ	ZZ	tt	DY	$W\gamma$	$W+\text{jet(s)}$	$gg \rightarrow H$	WH	ZH	VBF
Cross Section	<i>11.5%</i>	<i>11.5%</i>	<i>11.5%</i>	<i>10.0%</i>	5.0%	<i>10.0%</i>		<i>10.0%</i>	5.0%	5.0%	<i>10.0%</i>
Acceptance											
Scale (leptons)											
Scale (jets)								2.8%			
PDF Model (leptons)	1.9%	2.7%	2.7%	2.1%	4.1%	2.2%		-5.1%	1.2%	0.9%	2.2%
PDF Model (jets)								1.7%			
Higher-order Diagrams	5.5%	10.0%	10.0%	10.0%	5.0%	10.0%		-1.9%	<i>10.0%</i>	<i>10.0%</i>	<i>10.0%</i>
Missing Et Modeling	1.0%	1.0%	1.0%	1.0%	20.0%	1.0%		1.0%	1.0%	1.0%	1.0%
Conversion Modeling						20.0%					
Jet Fake Rates											
(Low S/B)											
(High S/B)											
MC Run Dependence	1.8%			2.2%		2.2%		2.6%	2.6%	1.9%	2.8%
Lepton ID Efficiencies	2.0%	2.0%	2.2%	1.8%	2.0%	2.0%		1.9%	1.9%	1.9%	1.9%
Trigger Efficiencies	2.1%	2.1%	2.1%	2.0%	3.4%	7.0%		3.3%	2.1%	2.1%	3.3%
Luminosity	3.8%	3.8%	3.8%	3.8%	3.8%	3.8%		3.8%	3.8%	3.8%	3.8%
Luminosity Monitor	4.4%	4.4%	4.4%	4.4%	4.4%	4.4%		4.4%	4.4%	4.4%	4.4%

TABLE XVII: Systematic uncertainties on the contributions for CDF's $H \rightarrow W^+W^- \rightarrow \ell^\pm \ell'^\mp$ channel with two or more jets. Systematic uncertainties are listed by name, see the original references for a detailed explanation of their meaning and on how they are derived. Systematic uncertainties for $gg \rightarrow H$ shown in this table are obtained for $m_H = 160 \text{ GeV}/c^2$. Uncertainties are relative, in percent and are symmetric unless otherwise indicated. Uncertainties in bold are correlated across jet bins but not across channels. Uncertainties in italics are correlated across jet bins and across appropriate channels.

Uncertainty Source	WW	WZ	ZZ	$t\bar{t}$	DY	$W\gamma$	$W+\text{jet(s)}$	$gg \rightarrow H$	WH	ZH	VBF
Cross Section	<i>11.5%</i>	<i>11.5%</i>	<i>11.5%</i>	<i>10.0%</i>	5.0%	<i>10.0%</i>		<i>10.0%</i>	<i>5.0%</i>	<i>5.0%</i>	<i>10.0%</i>
Acceptance											
Scale (leptons)								3.1%			
Scale (jets)								-8.7%			
PDF Model (leptons)	1.9%	2.7%	2.7%	2.1%	4.1%	2.2%		2.0%	1.2%	0.9%	2.2%
PDF Model (jets)								-2.8%			
Higher-order Diagrams	10.0%	10.0%	10.0%	10.0%	10.0%	10.0%		1.0%	<i>10.0%</i>	<i>10.0%</i>	<i>10.0%</i>
Missing Et Modeling	1.0%	1.0%	1.0%	1.0%	20.0%	1.0%			1.0%	1.0%	1.0%
Conversion Modeling						20.0%					
b -tag Veto				7.0%							
Jet Fake Rates							27.1%				
MC Run Dependence	1.0%			1.0%		1.0%		1.7%	2.0%	1.9%	2.6%
Lepton ID Efficiencies	1.9%	2.9%	1.9%	1.9%	1.9%	1.9%		1.9%	1.9%	1.9%	1.9%
Trigger Efficiencies	2.1%	2.1%	2.1%	2.0%	3.4%	7.0%		3.3%	2.1%	2.1%	3.3%
Luminosity	3.8%	3.8%	3.8%	3.8%	3.8%	3.8%		3.8%	3.8%	3.8%	3.8%
Luminosity Monitor	4.4%	4.4%	4.4%	4.4%	4.4%	4.4%		4.4%	4.4%	4.4%	4.4%

TABLE XVIII: Observed and expected limits for the $gg \rightarrow H \rightarrow W^+W^- \rightarrow \ell^+\nu_\ell\ell'^-\bar{\nu}_{\ell'}$ channel, with the high- s/b and low- s/b analyses combined, for all three jet categories. The observed and median expected limits are listed. Also listed are the limits from [3]. The limits are all given in units of $R = \sigma/\sigma_{SM}$, assuming SM branching fractions.

m_H (GeV/ c^2)	Observed limit/SM	median expected	CDF 9500 observed	CDF 9500 expected
100	191.6	133.83		
105	100.87	70.04		
110	57.3	40	57.89	38.90
115	20.32	19.24		
120	13.9	12.96	13.98	12.61
125	7.9	7.79		
130	6.11	6.05	6.13	6.05
135	4.66	4.62		
140	4.06	4.03	4.03	3.86
145	3.6	3.62	3.35	3.35
150	3.18	2.83	3.25	2.79
155	2.3	2.4	2.33	2.29
160	1.53	1.73	1.56	1.71
165	1.71	1.66	1.72	1.62
170	1.97	2.07	1.91	1.92
175	2.06	2.54	2.01	2.39
180	2.77	3.04	2.82	2.82
190	5.32	4.76	5.26	4.63
200	10.1	6.32	10.35	6.16

TABLE XIX: Systematic uncertainties on the contributions for CDF's $WH \rightarrow WWW \rightarrow \ell'^{\pm}\ell'^{\pm}$ channel. Systematic uncertainties are listed by name, see the original references for a detailed explanation of their meaning and on how they are derived. Uncertainties are relative, in percent and are symmetric unless otherwise indicated. An “s” is listed by a systematic uncertainty source if an accompanying shape uncertainty is assessed.

Uncertainty Source	Fakes	Conversions	WZ	ZZ	Signal
Fake Model	14.1s	0	0	0	0
JES	0	0	0s	0s	0s
Luminosity	0	0	4	4	4
Luminosity Monitor	0	0	5	5	5
Conversion Model	0	$^{+10.1}_{-7.0}$ s	0	0	0
Acceptance	0	0	2.2	2.7	1.5
Diboson Rate	0	0	11.5	11.5	0
FSR	0	0	0	0	5.5
ISR	0	0	0	0	5.2
PDF	0	0	0	0	2.7
W, Z + H Cross Section	0	0	0	0	5.0

TABLE XX: Observed and expected limits for the $W^\pm H \rightarrow W^\pm W^+ W^- \rightarrow \ell^\pm \nu_\ell \ell'^+ \nu_{\ell'} X$ channel, The observed and median expected limits are listed. Also listed are the limits from [14]. The limits are all given in units of $R = \sigma/\sigma_{SM}$, assuming SM branching fractions.

m_H (GeV/ c^2)	Observed limit/SM	median expected	CDF 7307 observed	CDF 7307 expected
110	291.61	181.01	283.0	180
115	112.73	68.80		
120	94.80	63.19	94.9	65
125	50.96	34.67		
130	61.76	35.49	60.9	36
135	45.24	26.42		
140	41.91	25.10	41.2	25
145	37.54	22.10		
150	39.39	21.50	38.7	22.0
155	39.16	21.33		
160	24.84	19.64	25.1	20.1
165	28.85	22.87		
170	36.28	23.24	36.7	24.0
175	46.46	29.54		
180	40.22	28.90	40.4	29
185	53.56	38.56		
190	49.52	33.42	49.2	34
195	63.12	42.54		
200	46.42	39.01	46.5	40

TABLE XXI: Observed and expected limits for all CDF SM Higgs boson search channels combined. The observed and median expected limits are listed, as well as $\pm 1, 2\sigma$ variation on the expected limits from statistical fluctuations assuming only background processes contribute. The limits are all given in units of $R = \sigma/\sigma_{SM}$, assuming SM branching fractions.

m_H (GeV/ c^2)	Observed limit/SM	-2σ expected	-1σ expected	median expected	$+1\sigma$ expected	$+2\sigma$ expected
100	2.70	1.42	1.87	2.63	3.77	5.33
105	2.58	1.46	1.93	2.65	3.66	4.99
110	3.50	1.48	2.03	2.88	4.07	5.62
115	3.76	1.62	2.21	3.17	4.54	6.36
120	4.10	2.06	2.71	3.72	5.13	6.97
125	4.91	2.13	2.82	3.89	5.41	7.41
130	4.67	2.15	2.93	4.12	5.80	8.00
135	4.26	2.01	2.70	3.82	5.43	7.58
140	4.11	1.94	2.60	3.61	5.02	6.86
145	3.96	1.85	2.52	3.5	4.84	6.55
150	3.48	1.51	1.95	2.7	3.78	5.24
155	2.50	1.26	1.68	2.34	3.29	4.54
160	1.56	0.92	1.24	1.75	2.47	3.43
165	1.76	0.91	1.23	1.72	2.41	3.32
170	2.05	1.09	1.45	2.01	2.80	3.85
175	2.12	1.30	1.78	2.5	3.48	4.75
180	2.88	1.51	2.14	3.02	4.20	5.69
190	5.57	2.52	3.32	4.61	6.44	8.85
200	9.98	3.39	4.54	6.33	8.85	12.14

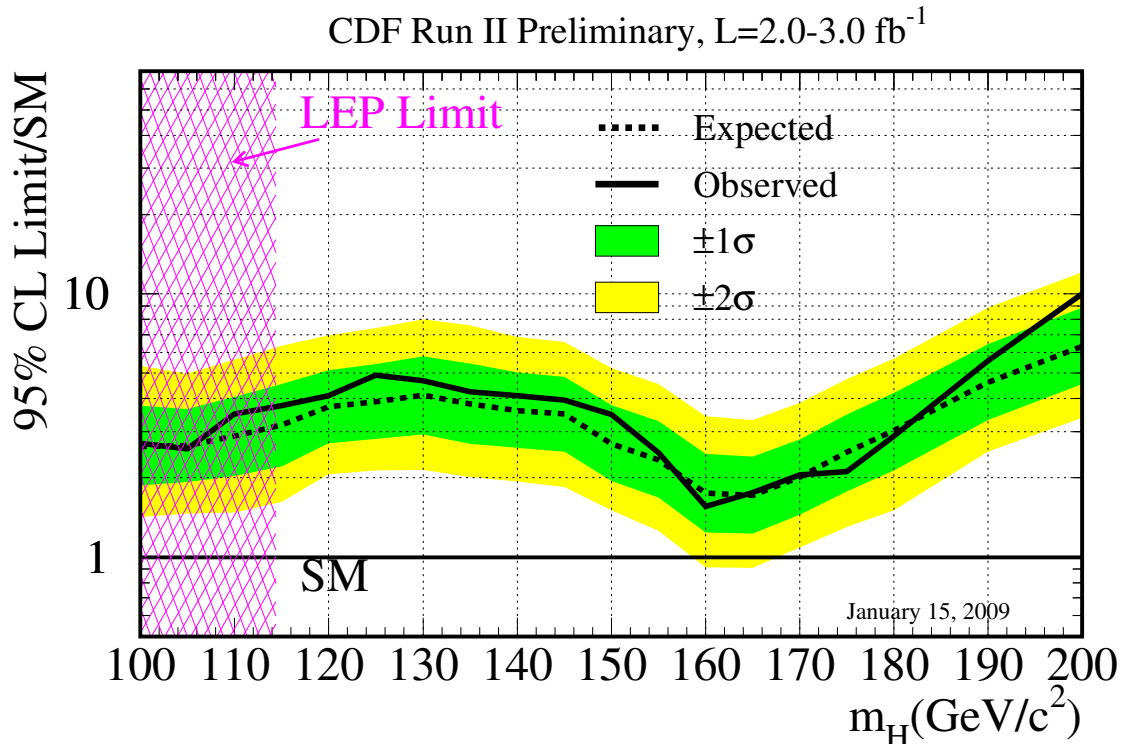


FIG. 1: The 95% CL upper limit on $R = \sigma/\sigma_{\text{SM}}$, shown as a function of m_H , for the combination of all of CDF's SM Higgs search channels. The $\pm 1, 2\sigma$ bands on the expected limits are also shown, centered on the median expected limit.

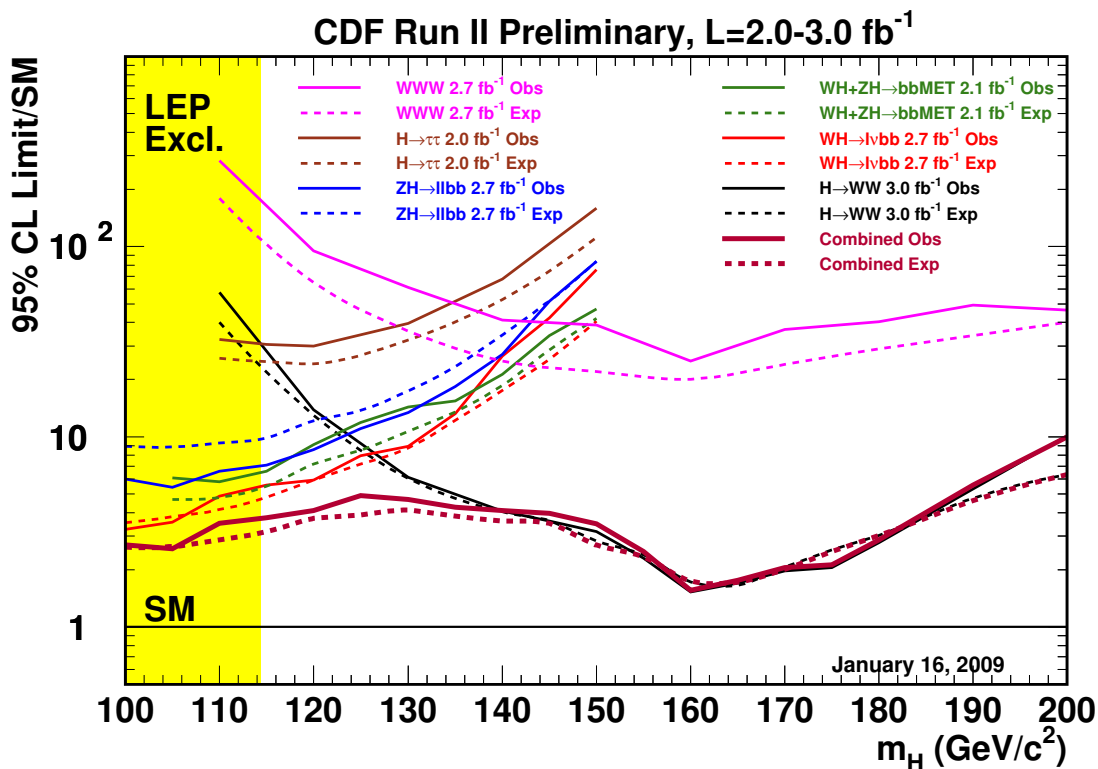


FIG. 2: The 95% CL upper limit on $R = \sigma/\sigma_{\text{SM}}$, shown as a function of m_H , shown separately for each analysis and for the combination. Dashed lines indicate the median expected limits, and the solid lines show the observed limits. The individual analysis limits are those approved by the individual analyses, and the combined limit is documented in this note. The LEP bound $m_H > 114.4 \text{ GeV}/c^2$ is shown in yellow.

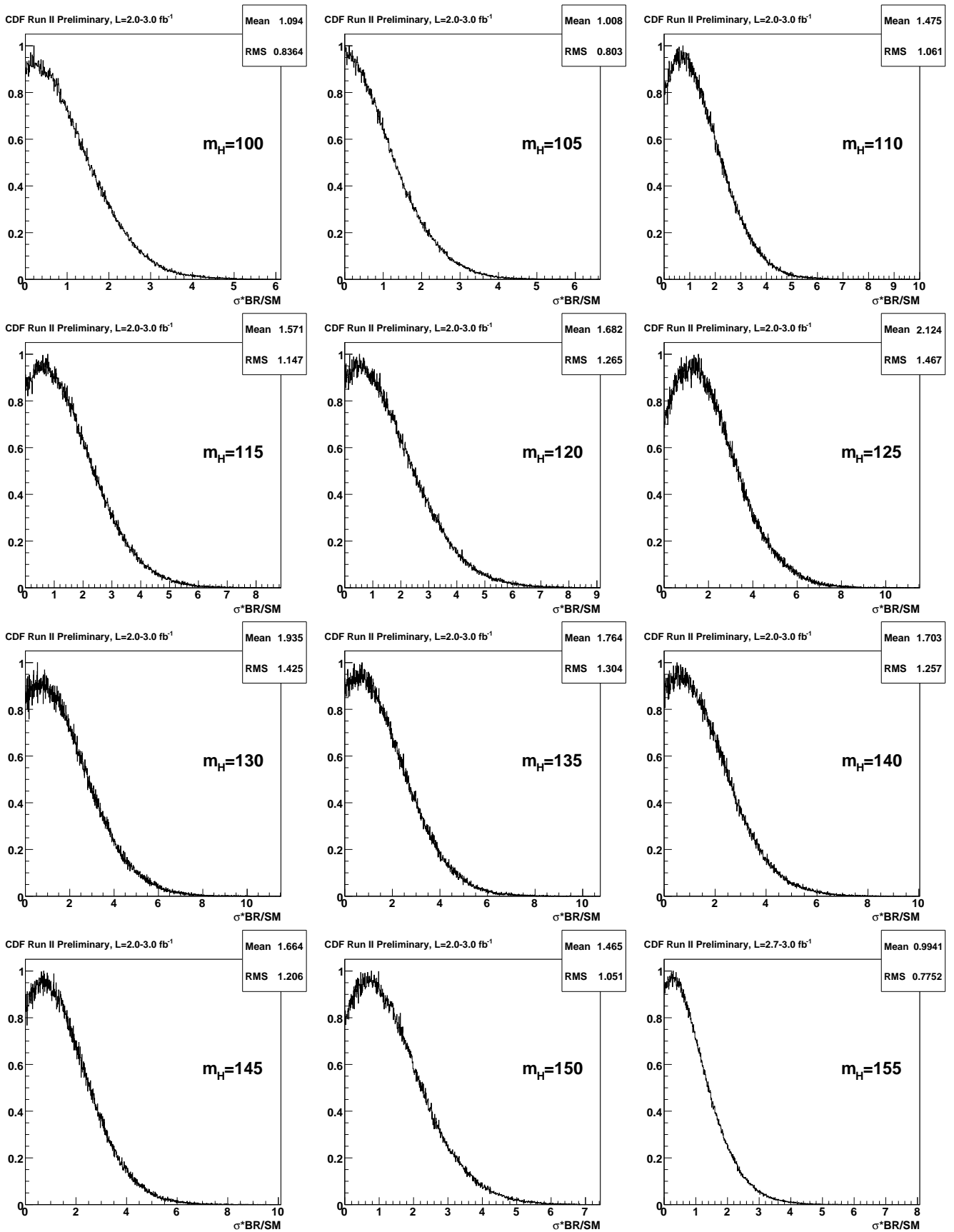


FIG. 3: The posterior densities and observed upper limits on $R = \sigma/\sigma_{SM}$, shown separately shown for Higgs boson masses of 100 through 155 GeV/c^2 .

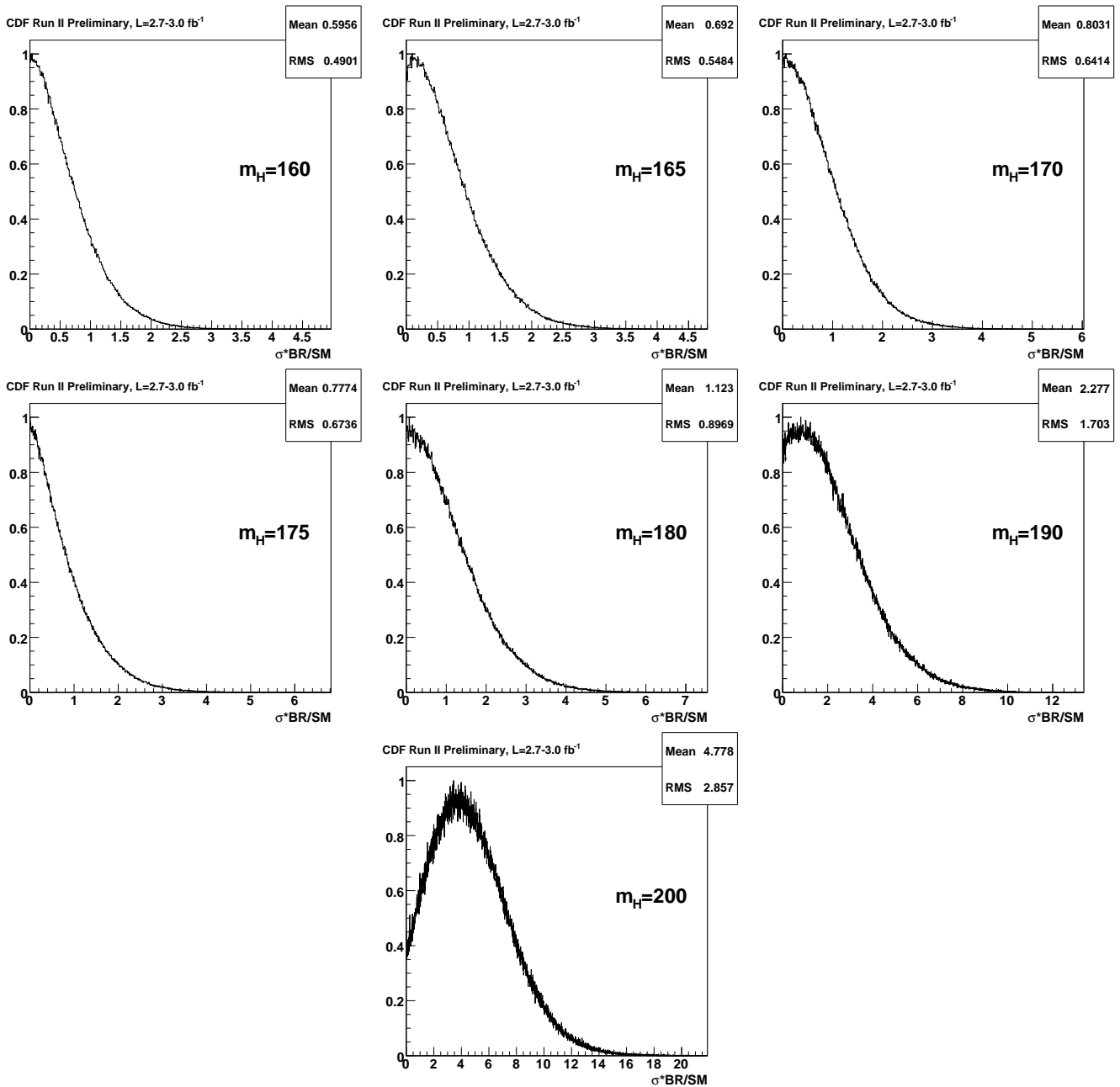


FIG. 4: The posterior densities and observed upper limits on $R = \sigma/\sigma_{SM}$, shown separately shown for Higgs boson masses of 160 through 200 GeV/c^2 .

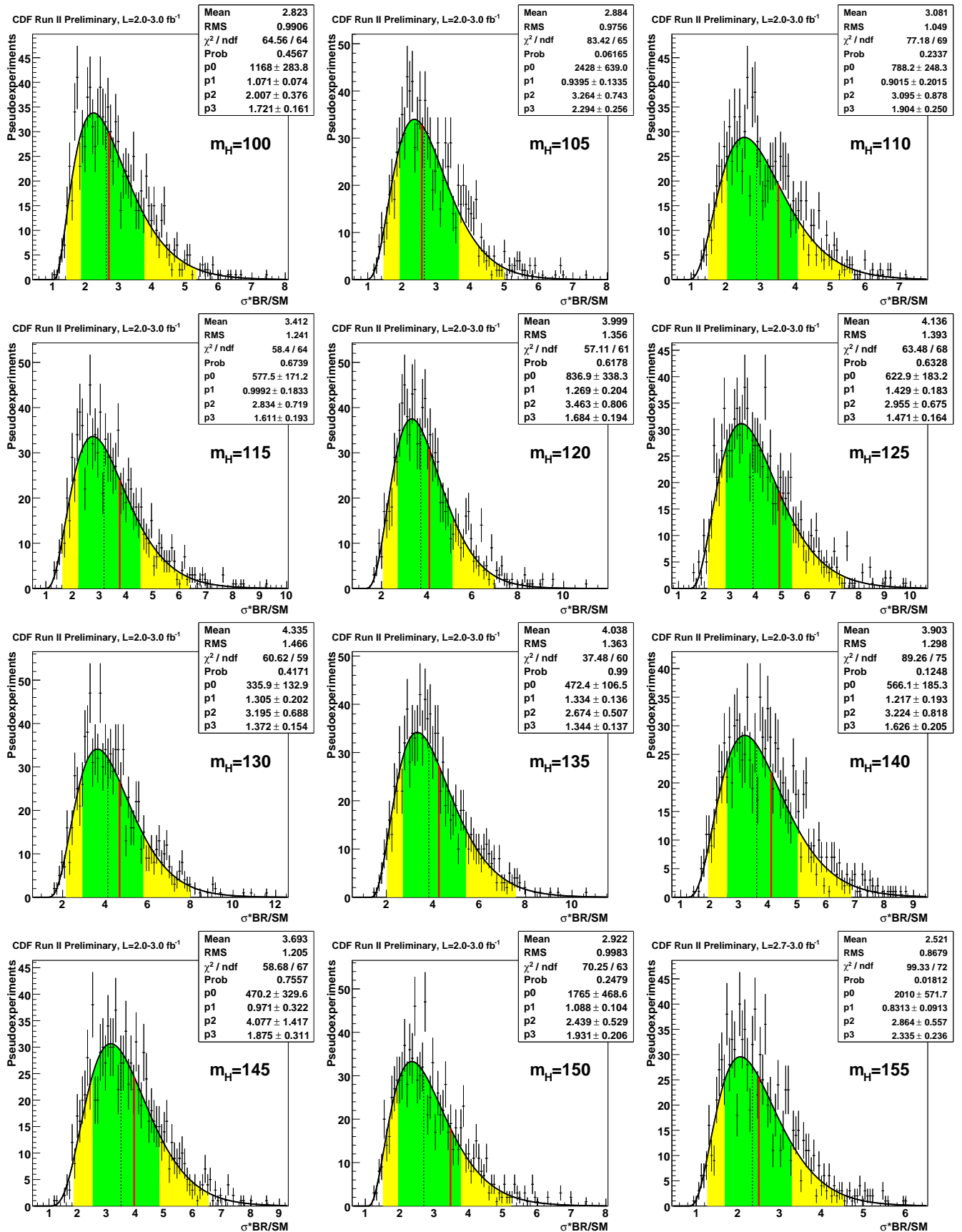


FIG. 5: The distributions of expected upper limits on $R = \sigma/\sigma_{\text{SM}}$ assuming no signal is truly present in the data, separately shown for Higgs boson masses of 100 through 155 GeV/c^2 .

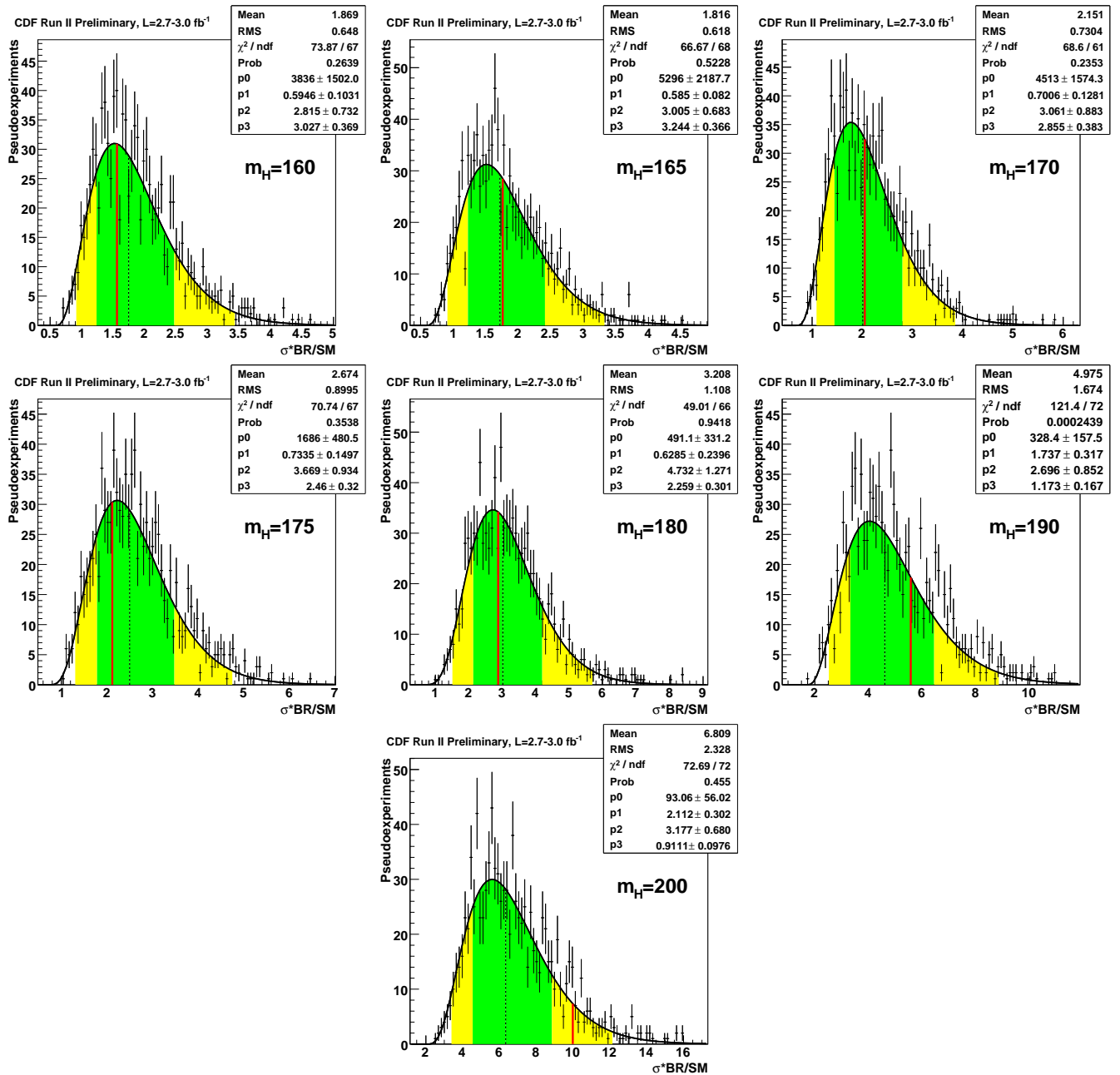


FIG. 6: The distributions of expected upper limits on $R = \sigma/\sigma_{\text{SM}}$ assuming no signal is truly present in the data, separately shown for Higgs boson masses of 160 through 200 GeV/c^2 .

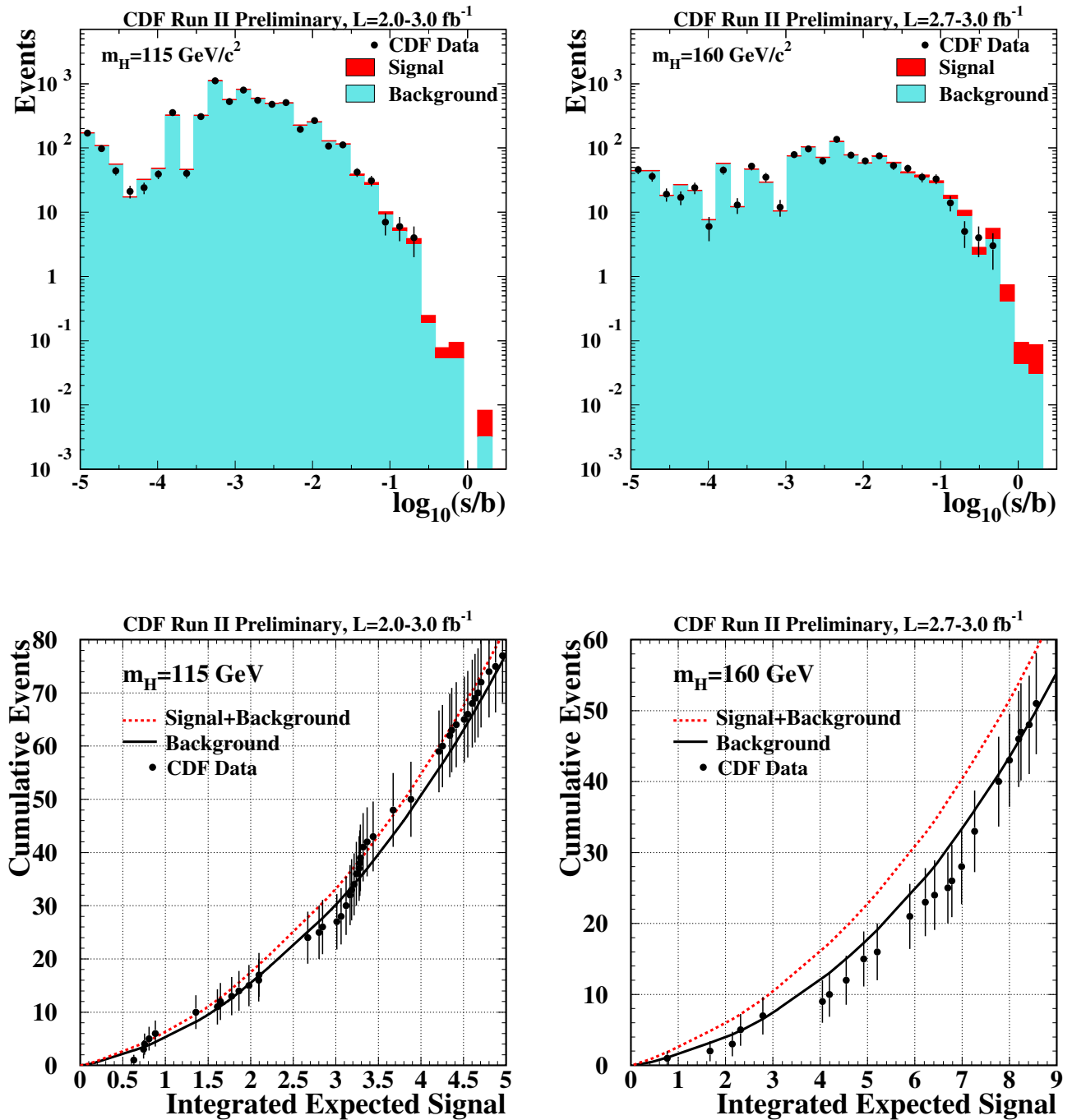


FIG. 7: Top plots: signal predictions, background predictions, and observed data, collected in bins sorted by s/b , for all channels added together. These are shown for $m_H=115$ and $160 \text{ GeV}/c^2$. Bottom plots: Integrated signal predictions, background predictions, and observed data, collected in bins sorted by s/b , for all channels added together. These are shown for $m_H=115$ and $160 \text{ GeV}/c^2$.

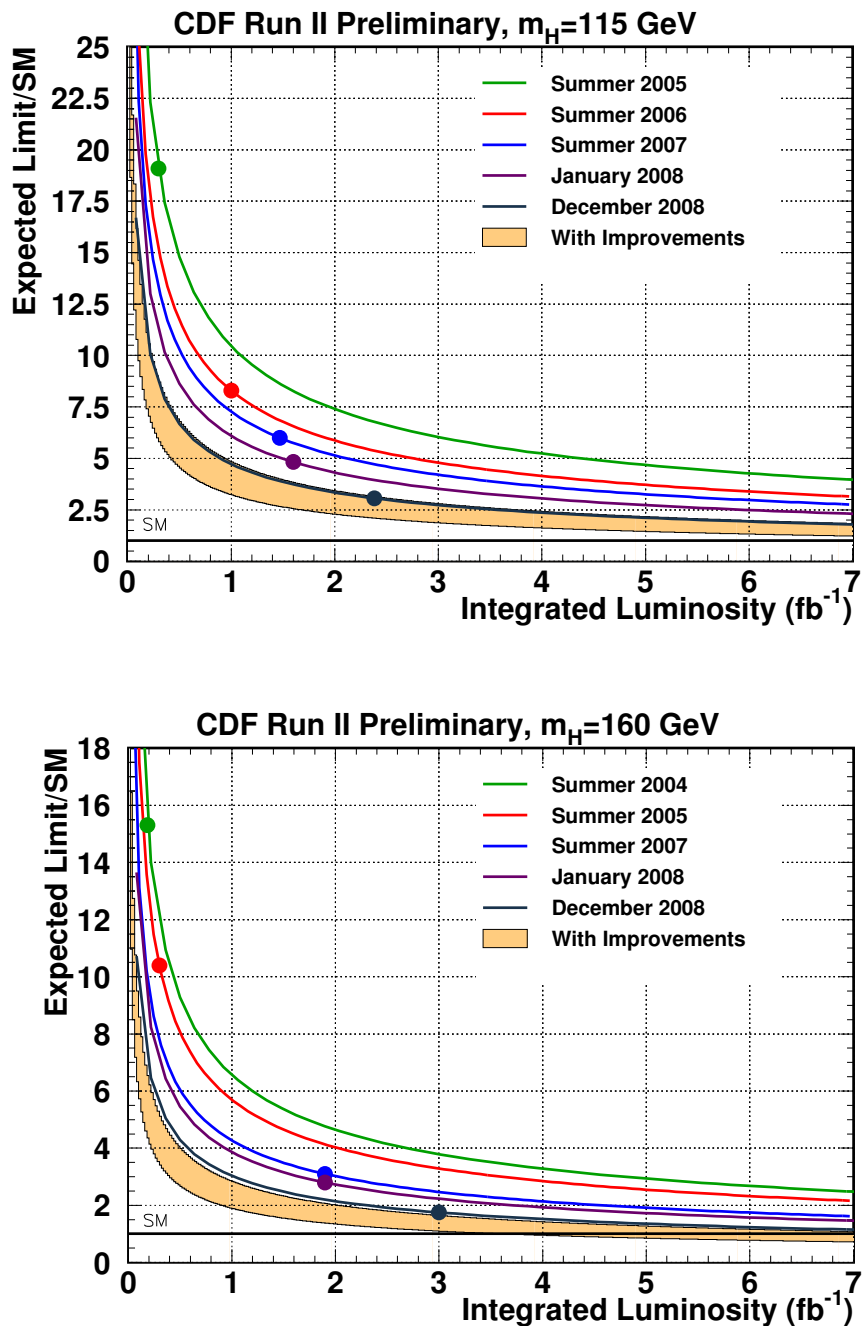


FIG. 8: Sensitivity projections and achieved sensitivities for the combined CDF Higgs boson searches, at $m_H = 115$ and $160 \text{ GeV}/c^2$. The curves are proportional to $1/\sqrt{\int L dt}$ extrapolations of the median expected limits, and each analysis update corresponds to a new point with a new curve. The light orange bands indicate ranges of possible improvements in performance, relative to the Summer 2007 sensitivity. The top of the light orange bands is a factor of 1.5 below the Summer 2007 curve, and the bottom of the light orange bands are a further factor of 1.5 below the top of the light orange bands.

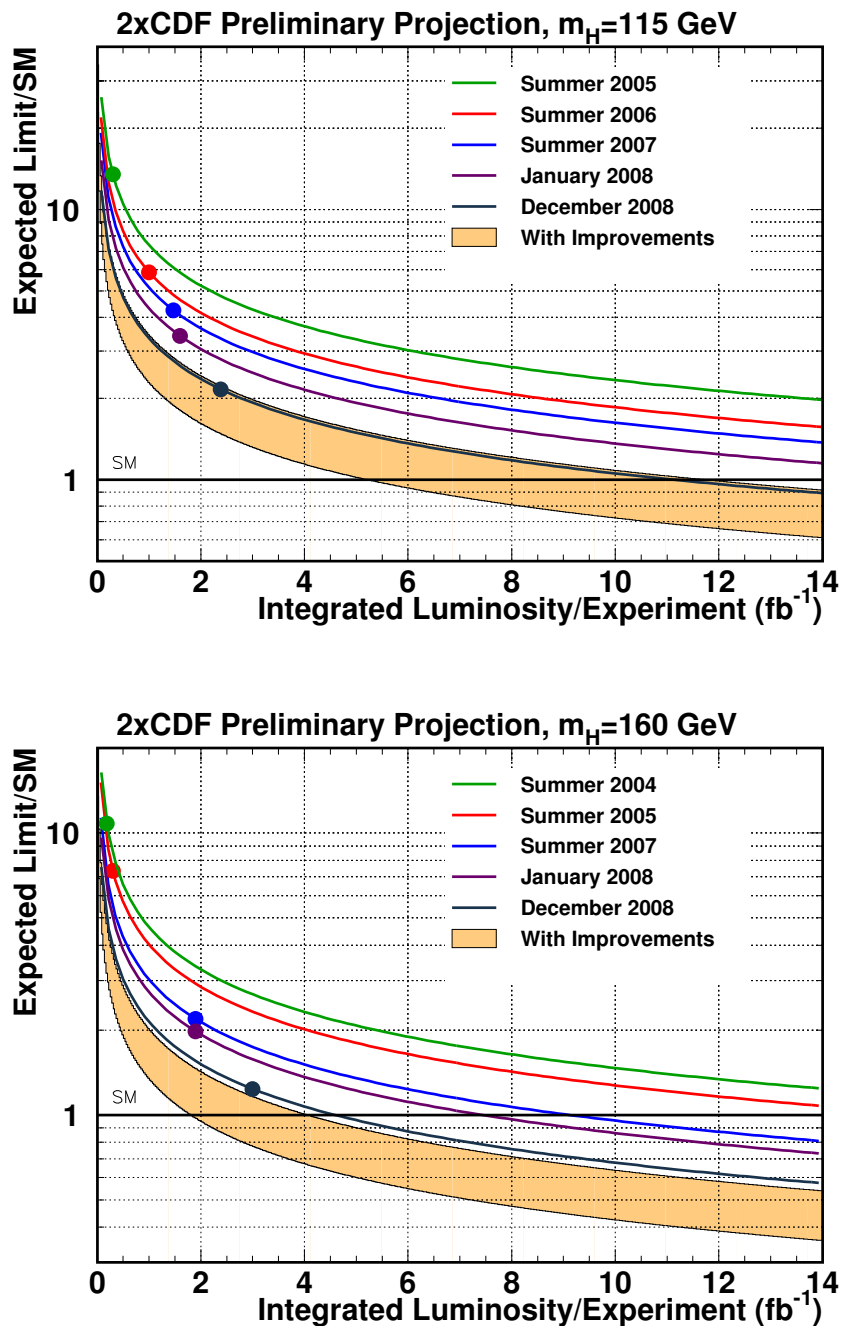


FIG. 9: Sensitivity projections and achieved sensitivities for the combined CDF Higgs boson searches, at $m_H = 115$ and 160 GeV/c^2 , with a multiplier of $1/\sqrt{2}$ applied to the expected limits, to approximate the contribution of D0, assuming identical performance. The curves are proportional to $1/\sqrt{\int L dt}$ extrapolations of the median expected limits, and each analysis update corresponds to a new point with a new curve. The light orange bands indicate ranges of possible improvements in performance, relative to the Summer 2007 sensitivity. The top of the light orange bands is a factor of 1.5 below the Summer 2007 curve, and the bottom of the light orange bands are a further factor of 1.5 below the top of the light orange bands. The points represent CDF's achieved sensitivities, where the expected limits have been divided by $\sqrt{2}$.

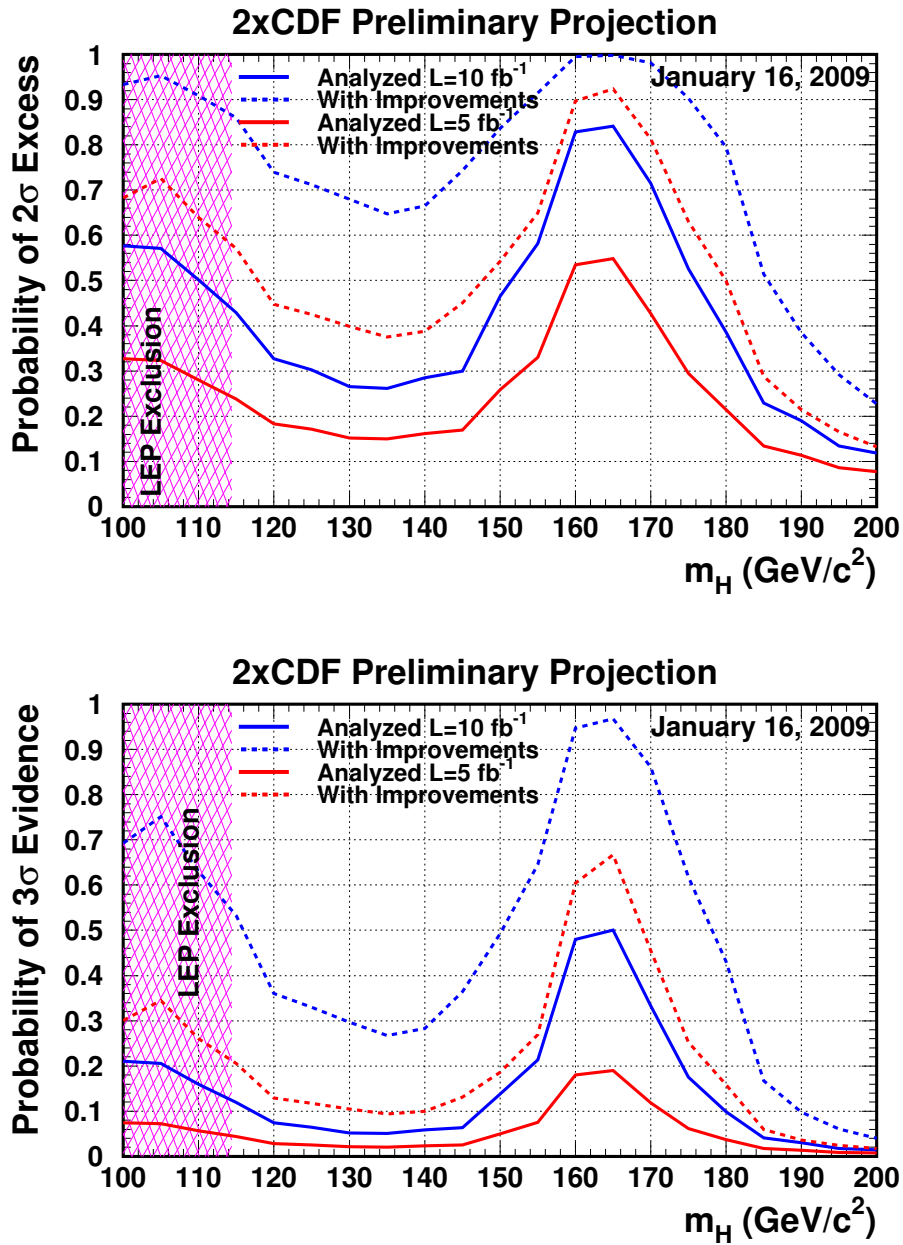


FIG. 10: Sensitivity projections as functions of m_H . These graphs show the chances of observing a 2σ excess (top) or a 3σ evidence (bottom), as functions of m_H , assuming a Higgs boson is present with production cross sections and decays at their SM values. CDF and D0 are assumed to contribute equally. The solid lines correspond to current performance as described in this note, and the dashed lines correspond to a performance level which corresponds to the bottom of the light orange bands in Figure 9. No account is taken of the data already collected and analyzed; existing excesses and deficits in the data do not affect these sensitivity projections. Two luminosity scenarios are considered: 5 fb^{-1} of analyzed luminosity per experiment (red lines) and 10 fb^{-1} of analyzed luminosity per experiment (blue lines).